Approaching Truly Freestanding Graphene: The Structure of Hydrogen-Intercalated Graphene on 6*H*-SiC(0001)

J. Sforzini,[1,2] L. Nemec,[3] T. Denig,[4] B. Stadtmüller,[1,2,*] T.-L. Lee,[5] C. Kumpf,[1,2] S. Soubatch,[1,2] U. Starke,[4] P. Rinke,[3,6] V. Blum,[3,7] F. C. Bocquet,[1,2,†] and F. S. Tautz[1,2]

[1]*Peter Grünberg Institut (PGI-3), Forschungszentrum Jülich, 52425 Jülich, Germany*
[2]*Jülich Aachen Research Alliance (JARA), Fundamentals of Future Information Technology, 52425 Jülich, Germany*
[3]*Fritz-Haber-Institut der Max-Planck-Gesellschaft, 14195 Berlin, Germany*
[4]*Max Planck Institute for Solid State Research, Heisenbergstraße, 70569 Stuttgart, Germany*
[5]*Diamond Light Source Ltd, Didcot, OX110DE Oxfordshire, United Kingdom*
[6]*COMP/Department of Applied Physics, Aalto University, P.O. Box 11100, Aalto FI-00076, Finland*
[7]*Department of Mechanical Engineering and Material Science, Duke University, Durham, North Carolina 27708, USA*

(Received 13 November 2014; published 10 March 2015)

We measure the adsorption height of hydrogen-intercalated quasifreestanding monolayer graphene on the (0001) face of 6*H* silicon carbide by the normal incidence x-ray standing wave technique. A density functional calculation for the full $(6\sqrt{3} \times 6\sqrt{3})$-*R*30° unit cell, based on a van der Waals corrected exchange correlation functional, finds a purely physisorptive adsorption height in excellent agreement with experiments, a very low buckling of the graphene layer, a very homogeneous electron density at the interface, and the lowest known adsorption energy per atom for graphene on any substrate. A structural comparison to other graphenes suggests that hydrogen-intercalated graphene on 6*H*-SiC(0001) approaches ideal graphene.

DOI: 10.1103/PhysRevLett.114.106804 PACS numbers: 73.20.Hb, 61.48.Gh, 68.49.Uv, 71.15.Mb

During the past decade, graphene attracted broad interest for its structural and electronic properties [1,2], which makes it a promising material for a wide range of applications, e.g., transistors in nanoscale devices [3] and energy storage [4]. The exact material properties of graphene depend on the growth conditions on a given substrate and its interaction with the substrate. In order to maintain its unique electronic properties, it is important to understand the coupling between the graphene layer and the substrate, in terms of covalent and noncovalent bonding, residual corrugation, and doping.

Large-scale ordered epitaxial graphene can be grown on various metal substrates. However, the metallic contact to the graphene layer determines its transport properties through, for instance, buckling or doping of the graphene layer [5,6]. It is therefore paramount to find a substrate for which the interactions are minimized in order to preserve the extraordinary properties of a single graphene layer. In addition, the use of a nonmetallic substrate is necessary to be able to use graphene, for instance, in electronic devices.

In this context, graphene growth on various faces of the wide band gap semiconductor silicon carbide (SiC) appears appealing. Riedl *et al.* [7] demonstrated the possibility to decouple graphene from SiC by intercalation of hydrogen atoms [quasifreestanding monolayer graphene (QFMLG)]. It is known from the band structure, core levels, and Raman spectroscopy of graphene [8,9] that the intercalation process reduces the interaction with the substrate substantially (removal of covalent bonds, less doping and strain). However, these measurements are indirect and, moreover, for weakly interacting graphenes the sensitivity of angle-resolved photoelectron spectroscopy (ARPES) becomes insufficient to assess the interaction with the substrate [10].

An alternative criterion to gauge the interaction strength of graphene with a substrate is its adsorption height. However, for hydrogen-intercalated graphene, the adsorption height is not known experimentally. Moreover, it is not clear whether for such a weakly interacting system this height can be calculated reliably as it is entirely determined by the van der Waals (vdW) interaction, which is difficult to treat. In this Letter, we present a density functional theory (DFT) calculation of QFMLG using the full unit cell and a vdW correction to the exchange correlation potential in which the dispersion coefficients are derived from the self-consistent electron density [11]. The calculation yields an adsorption height that is indicative of a purely vdW interaction. We validate this calculation with an accurate experimental height determination by normal incidence x-ray standing wave (NIXSW) and find an excellent agreement. By comparing our results to the adsorption height of graphene on various substrates taken from the literature, we demonstrate that QFMLG on SiC has the least graphene-substrate interaction among all studied systems. This is confirmed in our DFT calculations by a very low buckling of the graphene layer, a very

homogeneous electron density at the interface, and the lowest known adsorption energy per atom for graphene on any substrates.

Experiments and calculations were carried out for graphene on 6*H*-SiC(0001). Because of its smoothness and homogeneity, the Si-terminated surface of the 6*H*-SiC is widely used to achieve a controlled formation of high quality epitaxial graphene monolayers [12–15]. However, the first honeycomb carbon layer formed on the SiC(0001) surface consists of sp^2 and sp^3 hybridized orbitals leading to the formation of the so-called zero-layer graphene (ZLG) [16,17]. Since some of its atoms are covalently bonded to the Si atoms of the SiC surface, the ZLG does not show the typical Dirac cone in its band structure [8]. To recover the typical electronic properties of graphene, namely linear dispersion of the π and π^* bands at the K point of the hexagonal Brillouin zone, the formation of an additional graphene layer on top of the ZLG is required, generating epitaxial monolayer graphene (EMLG). Although the ZLG decouples the EMLG from the substrate, it is still considered to be a main obstacle for the development of graphene-based electronic devices because of the residual interactions. In fact, the Si dangling bonds in the top layer induce a significant doping in the EMLG even through the ZLG [18]. Replacing the carbon ZLG by a more passivating layer is therefore necessary to produce freestandinglike graphene on the SiC substrate. This can be achieved by hydrogen intercalation. The hydrogen atoms passivate the Si atoms in the top SiC bilayer. In this process the bonds between the ZLG and Si atoms are broken, the sp^3 atoms in the ZLG rehybridize, and the ZLG is lifted above the hydrogen atoms at the interface, forming QFMLG. Thus, hydrogen takes over the decoupling role of the ZLG layer in the EMLG.

The NIXSW experiments were performed in an ultrahigh vacuum end station at the I09 beam line at Diamond Light Source (Didcot, United Kingdom) equipped with a VG Scienta EW4000 hemispherical electron analyzer (acceptance angle of 60°) perpendicular to the incident beam direction. All data sets were recorded at room temperature and in a normal incidence geometry. A photon energy of approximately 2463 eV was used to excite the 6*H*-SiC(0006) reflection, which has a Bragg plane spacing of 2.517 Å. The NIXSW method, combining dynamical x-ray diffraction and photoelectron spectroscopy, is a powerful tool for determining the vertical adsorption distances at surfaces with sub-Å accuracy and high chemical sensitivity. The samples were prepared by thermal decomposition of SiC to produce the ZLG and then by annealing up to 700 °C in molecular hydrogen at atmospheric pressure to produce the QFMLG. After being transported in air to the beam line, the samples were outgassed in the end station before the x-ray measurements. ARPES using monochromatized He Iα radiation and low energy electron diffraction, shown in Ref. [19], were used to check the electronic and structural properties. The x-ray results were obtained from two samples at different spots and showed no sample and position dependence.

The surface SiC (C^{SiC}_{surf}) and graphene components of the C 1*s* spectrum are found at binding energies of 283.1 and 284.7 eV, respectively [Fig. 1(a)], and the Si 2*s* is found at 152.2 eV [Fig. 1(b)] for the surface SiC (Si^{SiC}_{surf}). The photoelectron yield of each chemical species is deduced from the peak area determined by a line-shape analysis of the core-level spectrum. This is repeated for all photon energy steps over a 2 eV range around the Bragg energy (E_{Bragg}) for all three species. Following a well-established procedure [19], we fit the final reflectivity and photoelectron yield curves with dynamical diffraction theory to determine the heights of the three different species with respect to the bulk-extrapolated SiC(0006) atomic plane. The C^{SiC}_{surf} atoms are located at 0.61 ± 0.04 Å below the bulk-extrapolated silicon plane and the Si^{SiC}_{surf} 0.05 ± 0.04 Å above. Thus, we obtain an experimental Si-C distance of 0.66 ± 0.06 Å, in agreement with the SiC crystalline structure [20,21]. In the same way, we find the adsorption height of the graphene layer with respect to the topmost Si layer to be 4.22 ± 0.06 Å, as shown in Fig. 2(a). We note that this height is approximately equal to the sum of the vdW radii of carbon and hydrogen (plus the Si-H distance of approximately 1.50 Å), and thus indicates the absence of interactions besides vdW.

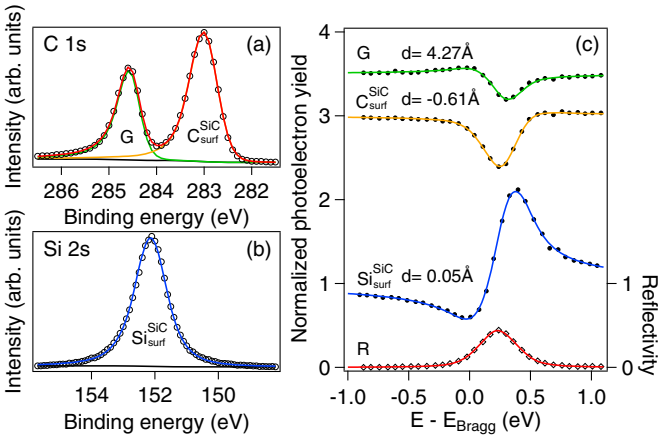

FIG. 1 (color online). NIXSW data measured for QFMLG on 6*H*-SiC(0001). (a) C 1*s* core level, fitted with two asymmetric Lorentzians. G and C^{SiC}_{surf} correspond to the graphene and the surface carbon atoms of SiC, respectively. (b) Si 2*p* core level fitted with a pseudo-Voigt function. Both were measured with a photon energy of 2494 eV. (c) Black dots show experimental photoelectron yield curves versus photon energy relative to the (0006) Bragg energy (2463 eV). The error bars, estimated according to Ref. [22], are smaller than the symbols. Fits to the yield curves for the surface atoms of SiC (Si^{SiC}_{surf}, C^{SiC}_{surf}) and graphene (G) are shown in blue, orange, and green, respectively [19,23–25]. The reflectivity R is plotted with black diamonds and its best fit in red. The absolute distances for each component are given with respect to the bulk-extrapolated silicon planes. The error bar for each value is ±0.04 Å.

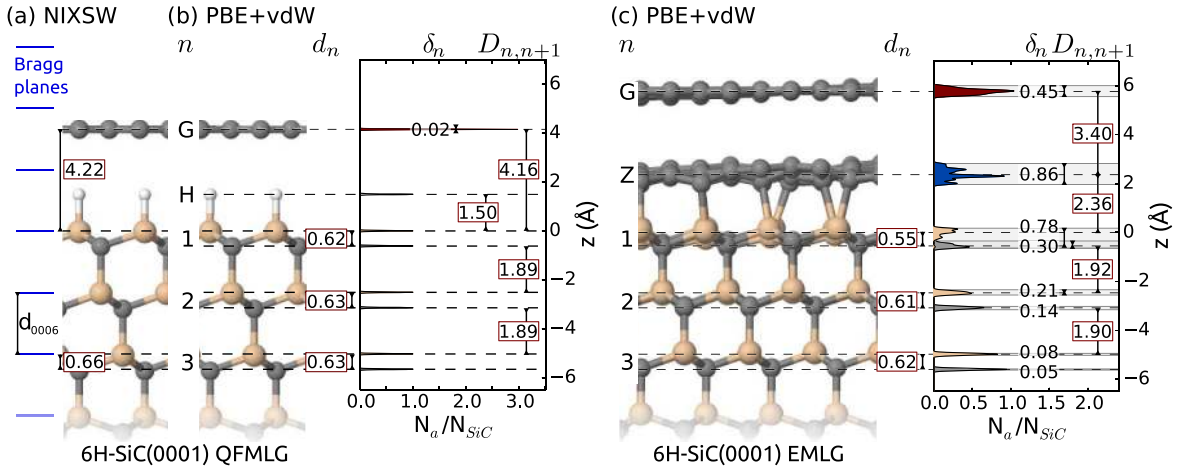

FIG. 2 (color online). (a) Vertical distances measured by NIXSW on QFMLG. The position of the Bragg planes around the surface are indicated by blue lines. PBE + vdW calculated geometry for (b) QFMLG and for (c) EMLG on 6*H*-SiC(0001) and histograms of the number of atoms N_a versus the atomic coordinates (z) relative to the topmost Si layer (Gaussian broadening: 0.02 Å). N_a is normalized by N_{SiC}, the number of SiC unit cells. $D_{n,n+1}$ is the distance between the layer n and $n+1$, d_n gives the Si-C distance within the SiC bilayer n, and δ_n is the corrugation of the layer n. All values are given in Å.

To test whether the structure of this predominantly vdW interacting interface can be predicted using DFT and to gain a detailed understanding of how hydrogen decouples the graphene layer from the substrate, we performed DFT calculations for the QFMLG and EMLG. The calculations were carried out using the all-electron, localized basis set code FHI-aims (tight settings) [26–29] and the Perdew-Burke-Ernzerhof (PBE) functional [30] with a correction for vdW effects (PBE + vdW). There are many different approaches to include long-range dispersion effects in DFT calculations [31]. We use the well-established Tkatchenko-Scheffler [11] method to efficiently include vdW effects in large-scale DFT calculations with thousands of atoms. It is a pairwise approach, where the effective C6 dispersion coefficients are derived from the self-consistent electron density. For the bulk lattice parameter of the 6*H*-SiC polytype, we find $a = 3.082$ Å and $c = 15.107$ Å. We stress that we investigate the QFMLG and EMLG reconstructions in the experimentally observed large commensurate $(6\sqrt{3} \times 6\sqrt{3})$-*R*30° supercell, almost strain-free (PBE + vdW: 0.1%) [32], consisting of 6 SiC bilayers under each surface reconstruction (1850 and 2080 atoms for the QFMLG and EMLG, respectively). We fully relaxed the top three SiC bilayers and all planes above (residual energy gradients $< 8 \times 10^{-3}$ eV/Å).

Figure 2 compares the measured structure of QFMLG [Fig. 2(a)] and the calculated structure of the QFMLG and EMLG [Figs. 2(b) and 2(c)] on 6*H*-SiC predicted at the PBE + vdW level. In addition, we include a histogram of the atomic z coordinates relative to the top Si layer normalized by the number of SiC unit cells. For illustration purposes, we broadened the histogram lines using a Gaussian with a width of 0.02 Å. For the QFMLG, we find a bulklike distance of 1.89 Å between the SiC bilayers. The Si-C distance within the top SiC bilayer (0.62 Å) and the remaining Si-C bilayer distances are practically bulklike (0.63 Å), in good agreement with the experimental result (0.66 ± 0.06 Å). The distance between the top Si layer and the graphene layer is 4.16 Å for 6*H*-SiC, again in good agreement with the measured 4.22 ± 0.06 Å. The 0.02 Å corrugation of the graphene layer is very small. For the hydrogen layer and all layers underneath, the corrugation is $< 10^{-2}$ Å.

The situation is very different for the EMLG in Fig. 2(c). Here a significant buckling of the graphene layer is observed [33,34]. In the EMLG, the interface between bulk SiC and graphene is formed by the partially covalently bonded ZLG. This interface layer is corrugated by 0.86 Å, leading to a buckling of the graphene layer of 0.45 Å, as well as a strong corrugation of 0.78 Å in the top Si layer. The interlayer distance (1.92 Å) between the top substrate bilayers is increased in comparison with the bulk value, while the Si-C distance within the topmost SiC bilayer is substantially reduced; see Fig. 2(c). In summary, our calculations provide a valid description of the graphene SiC interface, as they reproduce quantitatively the NIXSW-measured Si-graphene distances for both QFMLG and EMLG [32,33].

Using a smaller approximated $(\sqrt{3} \times \sqrt{3})$-*R*30° cell (50 atoms for QFMLG), we tested the influence of the exchange correlation functional and the type of vdW correction on the geometries [19]. The Si-graphene distance for QFMLG calculated in the approximated cell using the same methodology as discussed above is 4.25 Å. When we applied the highest level of theory using the Heyd-Scuseria-Ernzerhof hybrid functional (HSE06) [35] with a vdW correction incorporating many-body effects (HSE06 + MBD) [36–38], the Si-graphene distance increased slightly to 4.26 Å. The difference of 0.01 Å between PBE + vdW and HSE06 + MBD is negligible.

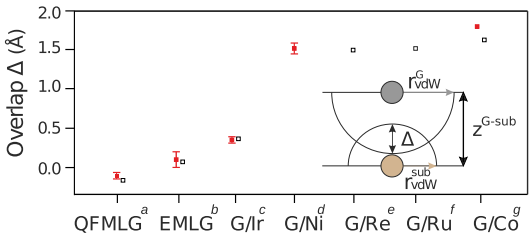

FIG. 3 (color online). Comparison of the overlap Δ for different epitaxial graphene systems. Δ is calculated by subtracting $z^{\mathrm{G-sub}}$ from the sum of graphene and substrate vdW radii. The empty and the filled squares correspond to DFT and measured values, respectively. (a) This work; (b) Refs. [32,33]; (c) Ref. [5]; (d) Ref. [6]; (e) Ref. [42]; (f) Ref. [43]; (g) Ref. [44].

We can thus conclude that changes in the predicted vertical structure of the $(6\sqrt{3}\times 6\sqrt{3})$-$R30°$ supercell would also be small even if higher-level approximations to the exchange correlation functional were employed.

Comparing the buckling of QFMLG (0.02 Å) and of EMLG (0.45 Å), we can conclude that QFMLG is much more ideal for device applications than EMLG. This is confirmed by a qualitative analysis in terms of overlapping vdW radii [39,40] where the overlap is defined by $\Delta = r^{\mathrm{G}}_{\mathrm{vdW}} + r^{\mathrm{sub}}_{\mathrm{vdW}} - z^{\mathrm{G-sub}}$ with $r^{\mathrm{G}}_{\mathrm{vdW}}$, $r^{\mathrm{sub}}_{\mathrm{vdW}}$, and $z^{\mathrm{G-sub}}$ being the vdW radii of graphene and of the atoms immediately below the graphene layer, and the measured distance between the graphene and the topmost atoms of the substrate, respectively. $\Delta > 0$ means that the vdW radii of the graphene and of the substrate overlap, indicating some degree of chemical interaction. On the other hand, for $\Delta \lesssim 0$, the graphene-substrate interaction is expected to be very weak. In Fig. 3, the overlap is plotted for QFMLG in comparison with other systems for which the adsorption heights have been measured or calculated. Epitaxial graphenes on SiC exhibit the lowest overlaps and QFMLG has by far the lowest value. This is also reflected in the low adsorption energy calculated for QFMLG, which is 59 meV/atom, significantly smaller than the corresponding values for EMLG (89.2 meV/atom) and graphite (81 meV/atom) [41].

Finally, we show that purely physisorptive adsorption with negligible buckling translates into a more decoupled electronic structure of the graphene. For this purpose, we calculate the change of electron density at the interface for QFMLG and EMLG. The calculations were performed with a 3*C*-SiC substrate as it allows us to use a smaller substrate thickness (4 layers instead of 6 for 6*H*-SiC) and renders the calculation more affordable. The SiC polytype (3*C* and 6*H*) is known not to influence the surface reconstructions [45,46]. We confirmed this by DFT for QFMLG and EMLG on both 6*H*-and 3*C*-SiC [19]. The electron density of the system is represented on an evenly distributed grid for the full system $\rho_{\mathrm{full}}(r)$. Similarly, the graphene layer $\rho_{\mathrm{G}}(r)$ and the substrate $\rho_{\mathrm{sub}}(r)$, calculated in isolation from each other, include the hydrogen layer for QFMLG and the ZLG for EMLG. The electron density difference $\Delta\rho(r)$ is given by $\Delta\rho(r) = \rho_{\mathrm{full}}(r) - [\rho_{\mathrm{G}}(r) + \rho_{\mathrm{sub}}(r)]$. Figure 4 shows

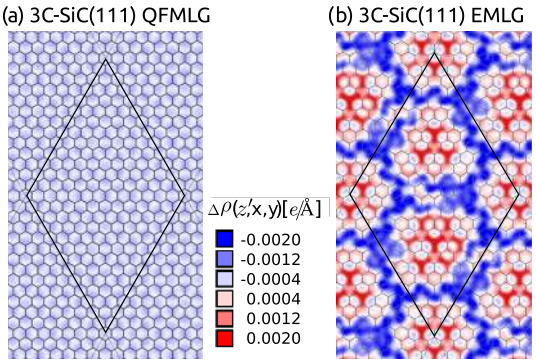

FIG. 4 (color online). Electron density differences $\Delta\rho(r) = \rho_{\mathrm{full}}(r) - [\rho_{\mathrm{G}}(r) + \rho_{\mathrm{sub}}(r)]$ for (a) 3*C*-SiC QFMLG and (b) 3*C*-SiC EMLG, calculated in the *x*-*y* plane between the substrate and the graphene layer (at $z' = 1.08$ Å below the graphene layer). The $(6\sqrt{3}\times 6\sqrt{3})$-$R30°$ supercell is shown in black and the graphene layer in gray.

$\Delta\rho(r)$ in the *x*-*y* plane at a given height between the substrate and the graphene layer. The resulting pattern is very similar for any chosen height [19]. In QFMLG, all Si atoms are saturated by hydrogen [47], resulting in negligible variations of the charge density within the *x*-*y* plane, as seen in Fig. 4(a). For EMLG, see Fig. 4(b), the electron density is modulated by the interplay of saturated and unsaturated Si bonds to the ZLG layer. The negligible $\Delta\rho(r)$ of QFMLG is an additional indication for the improved decoupling of the graphene layer from the substrate, thus preventing its buckling. This is in agreement with STM results [34] showing no corrugation within the experimental accuracy.

In conclusion, we have shown that DFT PBE + vdW calculations, for the large experimentally observed unit cell, accurately predict the adsorption height of QFMLG, in agreement with NIXSW measurements. QFMLG is the system having the largest adsorption distance among studied graphene-substrate systems; in particular, the overlap vanishes, suggesting a very effective decoupling of the graphene layer. Indeed, the calculations show that in comparison to EMLG, QFMLG is a very flat graphene layer with a very homogeneous electronic density at the interface. This significant difference translates into a dramatic improvement of transistors after hydrogen intercalation [48,49]. It suggests that the adsorption distance is a valid parameter to assess the ideality of graphene.

F. C. B. acknowledges financial support from the Initiative and Networking Fund of the Helmholtz Association, Postdoc Programme VH-PD-025. This research has been supported by the Academy of Finland through its Centres of Excellence Program (Project No. 251748). The authors would like to thank S. Schröder and C. Henneke for their support during the XSW beam-time, D. McCue for his excellent technical support at the I09 beam-line and B. Detlefs for helpful discussion.

*Present address: Department of Physics and Research Center OPTIMAS, University of Kaiserslautern, Erwin-Schrödinger-Strasse 46, 67663 Kaiserslautern, Germany.
†f.bocquet@fz-juelich.de

[1] Y. Zhang, Z. Jiang, J. P. Small, M. S. Purewal, Y.-W. Tan, M. Fazlollahi, J. D. Chudow, J. A. Jaszczak, H. L. Stormer, and P. Kim, Landau-Level Splitting in Graphene in High Magnetic Fields, Phys. Rev. Lett. **96**, 136806 (2006).

[2] M. I. Katsnelson, K. S. Novoselov, and A. K. Geim, Chiral tunnelling and the Klein paradox in graphene, Nat. Phys. **2**, 620 (2006).

[3] G. Fiori and G. Iannaccone, Multiscale modeling for graphene-based nanoscale transistors, Proc. IEEE **101**, 1653 (2013).

[4] D. Wang, R. Kou, D. Choi, Z. Yang, Z. Nie, J. Li, L. V. Saraf, D. Hu, J. Zhang, G. L. Graff, J. Liu, M. A. Pope, and I. A. Aksay, Ternary self-assembly of ordered metal oxide-graphene nanocomposites for electrochemical energy storage, ACS Nano **4**, 1587 (2010).

[5] C. Busse, P. Lazić, R. Djemour, J. Coraux, T. Gerber, N. Atodiresei, V. Caciuc, R. Brako, A. T. NDiaye, S. Blügel, J. Zegenhagen, and T. Michely, Graphene on Ir(111): Physisorption with Chemical Modulation, Phys. Rev. Lett. **107**, 036101 (2011).

[6] Y. Gamo, A. Nagashima, M. Wakabayashi, M. Terai, and C. Oshima, Atomic structure of monolayer graphite formed on Ni(111), Surf. Sci. **374**, 61 (1997).

[7] C. Riedl, C. Coletti, T. Iwasaki, A. A. Zakharov, and U. Starke, Quasi-Free-Standing Epitaxial Graphene on SiC Obtained by Hydrogen Intercalation, Phys. Rev. Lett. **103**, 246804 (2009).

[8] S. Forti and U. Starke, Epitaxial graphene on SiC: from carrier density engineering to quasi-free standing graphene by atomic intercalation, J. Phys. D **47**, 094013 (2014).

[9] F. Speck, J. Jobst, F. Fromm, M. Ostler, D. Waldmann, M. Hundhausen, H. B. Weber, and T. Seyller, The quasi-free-standing nature of graphene on H-saturated SiC(0001), Appl. Phys. Lett. **99**, 122106 (2011).

[10] J. C. Johannsen, S. Ulstrup, M. Bianchi, R. Hatch, D. Guan, F. Mazzola, L. Hornekr, F. Fromm, C. Raidel, T. Seyller, and P. Hofmann, Electron-phonon coupling in quasi-free-standing graphene, J. Phys. Condens. Matter **25**, 094001 (2013).

[11] A. Tkatchenko and M. Scheffler, Accurate Molecular Van Der Waals Interactions from Ground-State Electron Density and Free-Atom Reference Data, Phys. Rev. Lett. **102**, 073005 (2009).

[12] I. Forbeaux, J.-M. Themlin, and J.-M. Debever, Heteroepitaxial graphite on 6H—SiC(0001): Interface formation through conduction-band electronic structure, Phys. Rev. B **58**, 16396 (1998).

[13] K. V. Emtsev, A. Bostwick, K. Horn, J. Jobst, G. L. Kellogg, L. Ley, J. L. McChesney, T. Ohta, S. A. Reshanov, J. Röhrl, E. Rotenberg, A. K. Schmid, D. Waldmann, H. B. Weber, and T. Seyller, Towards wafer-size graphene layers by atmospheric pressure graphitization of silicon carbide, Nat. Mater. **8**, 203 (2009).

[14] U. Starke and C. Riedl, Epitaxial graphene on SiC(0001) and $SiC(000\bar{1})$: from surface reconstructions to carbon electronics, J. Phys. Condens. Matter **21**, 134016 (2009).

[15] C. Riedl, C. Coletti, and U. Starke, Structural and electronic properties of epitaxial graphene on SiC(0 0 0 1): a review of growth, characterization, transfer doping and hydrogen intercalation J. Phys. D **43**, 374009 (2010).

[16] F. Varchon, R. Feng, J. Hass, X. Li, B. N. Nguyen, C. Naud, P. Mallet, J.-Y. Veuillen, C. Berger, E. H. Conrad, and L. Magaud, Electronic Structure of Epitaxial Graphene Layers on SiC: Effect of the Substrate, Phys. Rev. Lett. **99**, 126805 (2007).

[17] K. V. Emtsev, F. Speck, T. Seyller, L. Ley, and J. D. Riley, Interaction, growth, and ordering of epitaxial graphene on $SiC\{0001\}$ surfaces: A comparative photoelectron spectroscopy study, Phys. Rev. B **77**, 155303 (2008).

[18] A. Bostwick, T. Ohta, J. L. McChesney, K. V. Emtsev, T. Seyller, K. Horn, and E. Rotenberg, Symmetry breaking in few layer graphene films, New J. Phys. **9**, 385 (2007).

[19] See Supplemental Material at http://link.aps.org/supplemental/10.1103/PhysRevLett.114.106804 for APRES and LEED data used to check the electronic and structural properties of the samples presented in this work. More details about the NIXSW technique are introduced. In addition, we include structural details calculated in the approximated $\sqrt{3} \times \sqrt{3}$-$R30°$ cell using different approximations to the exchange correlation functionals and van der Waals treatment.

[20] B. Lee, S. Han, and Y.-S. Kim, First-principles study of preferential sites of hydrogen incorporated in epitaxial graphene on 6H-SiC(0001), Phys. Rev. B **81**, 075432 (2010).

[21] J. Wang, L. Zhang, Q. Zeng, G. L. Vignoles, and L. Cheng, Surface relaxation and oxygen adsorption behavior of different SiC polytypes: a first-principles study, J. Phys. Condens. Matter **22**, 265003 (2010).

[22] G. Mercurio, O. Bauer, M. Willenbockel, N. Fairley, W. Reckien, C. H. Schmitz, B. Fiedler, S. Soubatch, T. Bredow, M. Sokolowski, and F. S. Tautz, Adsorption height determination of nonequivalent C and O species of PTCDA on Ag(110) using x-ray standing waves, Phys. Rev. B **87**, 045421 (2013).

[23] D. P. Woodruff, Normal incidence X-ray standing wave determination of adsorbate structures, Prog. Surf. Sci. **57**, 1 (1998).

[24] D. P. Woodruff, Surface structure determination using x-ray standing waves, Rep. Prog. Phys. **68**, 743 (2005).

[25] I. A. Vartanyants and M. V. Kovalchuk, Theory and applications of x-ray standing waves in real crystals, Rep. Prog. Phys. **64**, 1009 (2001).

[26] V. Blum, R. Gehrke, F. Hanke, P. Havu, V. Havu, X. Ren, K. Reuter, and M. Scheffler, Ab initio molecular simulations with numeric atom-centered orbitals, Comput. Phys. Commun. **180**, 2175 (2009).

[27] V. Havu, V. Blum, P. Havu, and M. Scheffler, Efficient O (N) integration for all-electron electronic structure calculation using numeric basis functions, J. Comput. Phys. **228**, 8367 (2009).

[28] T. Auckenthaler, V. Blum, H. Bungartz, T. Huckle, R. Johanni, L. Krämer, B. Lang, H. Lederer, and P. Willems, Parallel solution of partial symmetric eigenvalue problems from electronic structure calculations, Parallel Comput. **37**, 783 (2011).

[29] X. Ren, P. Rinke, V. Blum, J. Wieferink, A. Tkatchenko, A. Sanfilippo, K. Reuter, and M. Scheffler, Resolution-of-identity approach to Hartree-Fock, hybrid density functionals, RPA, MP2 and GW with numeric atom-centered orbital basis functions, New J. Phys. **14**, 053020 (2012).

[30] J. P. Perdew, K. Burke, and M. Ernzerhof, Generalized Gradient Approximation Made Simple (vol 77, Pg 3865, 1996), Phys. Rev. Lett. **78**, 1396 (1997).
[31] J. F. Dobson and T. Gould, Calculation of dispersion energies, J. Phys. Condens. Matter **24**, 073201 (2012).
[32] L. Nemec, V. Blum, P. Rinke, and M. Scheffler, Thermodynamic Equilibrium Conditions of Graphene Films on SiC, Phys. Rev. Lett. **111**, 065502 (2013).
[33] J. D. Emery, B. Detlefs, H. J. Karmel, L. O. Nyakiti, D. K. Gaskill, M. C. Hersam, J. Zegenhagen, and M. J. Bedzyk, Chemically Resolved Interface Structure of Epitaxial Graphene on SiC(0001), Phys. Rev. Lett. **111**, 215501 (2013).
[34] S. Goler, C. Coletti, V. Piazza, P. Pingue, F. Colangelo, V. Pellegrini, K. V. Emtsev, S. Forti, U. Starke, F. Beltram, and S. Heun, Revealing the atomic structure of the buffer layer between SiC(0001) and epitaxial graphene, Carbon **51**, 249 (2013).
[35] A. V. Krukau, O. A. Vydrov, A. F. Izmaylov, and G. E. Scuseria, Influence of the exchange screening parameter on the performance of screened hybrid functionals, J. Chem. Phys. **125**, 224106 (2006).
[36] A. Ambrosetti, A. M. Reilly, R. A. DiStasio, and A. Tkatchenko, Long-range correlation energy calculated from coupled atomic response functions, J. Chem. Phys. **140**, 18A508 (2014).
[37] A. Tkatchenko, A. Ambrosetti, and R. A. DiStasio, Interatomic methods for the dispersion energy derived from the adiabatic connection fluctuation-dissipation theorem, J. Chem. Phys. **138**, 074106 (2013).
[38] A. Tkatchenko, R. A. DiStasio, R. Car, and M. Scheffler, Accurate and Efficient Method for Many-Body van der Waals Interactions, Phys. Rev. Lett. **108**, 236402 (2012).
[39] A. Bondi, van der Waals volumes and radii, J. Phys. Chem. **68**, 441 (1964).
[40] S. Batsanov, Van der Waals radii of elements, Inorg. Mater. (USSR) **37**, 871 (2001).
[41] In Ref [5], a value of 50 meV/atom has been found for graphene on Ir(111). However, this value is an average over a chemically modulated physisorbed graphene layer. Hence, parts of the layer have a much larger adsorption energy.
[42] E. Miniussi, M. Pozzo, A. Baraldi, E. Vesselli, R. R. Zhan, G. Comelli, T. O. Mentes, M. A. Niño, A. Locatelli, S. Lizzit, and D. Alfè, Thermal Stability of Corrugated Epitaxial Graphene Grown on Re(0001), Phys. Rev. Lett. **106**, 216101 (2011).
[43] B. Wang, S. Günther, J. Wintterlin, and M.-L. Bocquet, Periodicity, work function and reactivity of graphene on Ru(0001) from first principles, New J. Phys. **12**, 043041 (2010).
[44] D. Eom, D. Prezzi, K. T. Rim, H. Zhou, M. Lefenfeld, S. Xiao, C. Nuckolls, M. S. Hybertsen, T. F. Heinz, and G. W. Flynn, Structure and electronic properties of graphene nanoislands on Co(0001), Nano Lett. **9**, 2844 (2009).
[45] J. Schardt, J. Bernhardt, U. Starke, and K. Heinz, Crystallography of the (3×3) surface reconstruction of 3C-SiC (111), 4H-SiC(0001), and 6H-SiC(0001) surfaces retrieved by low-energy electron diffraction, Phys. Rev. B **62**, 10335 (2000).
[46] O. Pankratov, S. Hensel, P. Götzfried, and M. Bockstedte, Graphene on cubic and hexagonal SiC: A comparative theoretical study, Phys. Rev. B **86**, 155432 (2012).
[47] F. C. Bocquet, R. Bisson, J.-M. Themlin, J.-M. Layet, and T. Angot, Reversible hydrogenation of deuterium-intercalated quasi-free-standing graphene on SiC(0001), Phys. Rev. B **85**, 201401 (2012).
[48] S. Hertel, D. Waldmann, J. Jobst, A. Albert, M. Albrecht, S. Reshanov, A. Schöner, M. Krieger, and H. B. Weber, Tailoring the graphene/silicon carbide interface for monolithic wafer-scale electronics, Nat. Commun. **3**, 957 (2012).
[49] F.-H. Liu, S.-T. Lo, C. Chuang, T.-P. Woo, H.-Y. Lee, C.-W. Liu, C.-I. Liu, L.-I. Huang, C.-H. Liu, Y. Yang, C.-Y. S. Chang, L.-J. Li, P. C. Mende, R. M. Feenstra, R. E. Elmquist, and C.-T. Liang, Hot carriers in epitaxial graphene sheets with and without hydrogen intercalation: role of substrate coupling, Nanoscale **6**, 10562 (2014).